Co-published by
Institute of Fluid-Flow Machinery
Polish Academy of Sciences
Committee on Thermodynamics and Combustion
Polish Academy of Sciences

Copyright©2026 by the Authors under licence CC BY-NC-ND 4.0

http://www.imp.gda.pl/archives-of-thermodynamics/

A novel passive solar energy space heating design of an emergency tent

Aed Ibrahim Owaid*, Sabah M. Hadi, Husam Sabeeh Al-Arab

Scientific Research Commission, Baghdad, Iraq
*Corresponding author email: aedaltaher@gmail.com

Received: 26.02.2026; revised: 09.07.2026; accepted: 21.07.2026

Abstract

The adjustable tent is utilised in construction sites, military camps, tourist locations, disaster relief efforts, rescue operations, nomadic living, and other situations. Current methods offer thermal comfort in tents but may elevate weight, expense and complexity. This study introduces a design for a passive solar heating tent that controls internal temperatures using renewable solar energy. This tent was designed using SolidWorks, featuring a Nylon 6.6 cover and a metal frame. The study's results indicate that the aperture area of the sun's trajectory is essential for the tent's energy harvesting capability. The design's principal characteristic is the rectangular prism-shaped air containers, comprising three passive solar containers (PSAC) and two insulation containers (ISC). These containers (PSAC and ISC) can be utilised during the winter and stored during the summer. To determine the minimum necessary aperture area, we computed the tent's maximum thermal losses, representing the required space heating load of 1000 W. We formulated an equation to determine the aperture area of the three-sided tent on the sun-exposed sides based on the azimuth and elevation angles that affect the solar collectors. The integration of the five containers (PSAC and ISC) with the tent enhances thermal insulation by reducing the heat transfer coefficient from 6.5 W/(m^2·K) to 0.168 W/(m^2·K).

Keywords: Passive solar heating; Rectangular prism-shaped air containers; Air containers; Emergency tent; SolidWorks.

Vol. 47(2026), No. 3, 69–77; doi: 10.24425/ather.2026.3655

Cite this manuscript as: Owaid, A.I., Hadi, S.M., & Al-Arab, H.S. (2026). A novel passive solar energy space heating design of an emergency tent. *Archives of Thermodynamics*, 47(3), 69−77.

1. Introduction

Since the dawn of civilisation, humans have created and employed tents constructed from natural materials. These tents function as a critical form of emergency shelter [1]. The International Federation of Red Cross and Red Crescent Societies (IFRC) continuously invests in upgrading tents [2], pointing out the significance of tents as essential tools in the initial phases of humanitarian assistance. Temporary shelters must be used when calamities strike, and there are not enough facilities to house the displaced. Shelter is a human right and a necessity for the population's physical and mental well-being [3].

The unstable global situation, changing weather and climate conditions, medical risks, and natural disasters have necessitated the need for temporary housing alternatives for the affected population. In addition, well over 42 million individuals have been forcibly displaced due to conflicts over the past decade, while 2.9 billion people have been affected by natural disasters in the first twelve years of this century [4−6]. Relief organisations, as international aid is estimated in 2019, offer emergency shelter to numerous affected individuals [7,8].

Thermal comfort refers to being content with ambient temperatures. The absence of adverse sensations associated with heat impacts is also assessed. Thermal comfort necessitates a ba-

Nomenclature

A – area, m^2
EoT– equation of time
F – factor
h – convection heat transfer coefficient, $W/(m^2 \cdot K)$
H – heat gain, W
I – rate of solar radiation, W/m^2
K – thermal conductivity, $W/(m \cdot K)$
l – window length, m
L – tent length, m
Lat – latitude, °
Lon– longitude, °
LT – local time, s
n – number of the day within the year
N – number of persons
Q – power, W
$\dot{Q}$ – heat flow rate, W
R – thermal resistance, $(m^2 \cdot K)/W$
ST – solar time
STM– standard time meridian, °
th – time hour angle, °
T – temperature, °C
U – overall heat transfer coefficient, $W/(m^2 \cdot K)$
$\dot{V}$ – volumetric air flow rate, m^3/s
w – window height, m
W – tent height, m
Z – azimuth angle, °

Greek symbols

α – elevation angle, °
δ – declination, °
η – conversion efficiency of the black paint

Subscripts and Superscripts

a – aperture
am – ambient
c – cross section
e – equipment
ex – external
$gain$– gain
h – harvested energy
hg – heat gain
i – internal static air
in – internal
inf – infiltration
l – latent
$loss$ – heat losses
o – outer moving air
P – persons
r – required power
S – sensible
sp – space
t – total
u – usage

Abbreviations and Acronyms

CLF – cooling load factor
CPVC– chlorinated polyvinyl chloride
IAC – insulation air containers
PMV – predicted mean vote
PPD – predicted percentage of dissatisfied
PSAC– passive solar air containers

lance between body heat production and loss [9–11]. The predicted mean vote (PMV) and predicted percentage of dissatisfied (PPD) indices are frequently employed to assess thermal comfort; however, some studies [12,13] suggest that the PPD index may not adequately represent individual perceptions in hot and humid environments, and PMV-PPD models exhibit certain limitations. Yang et al. [14] performed a supplementary study in Tianjin to corroborate this assertion. Environmental elements and tent attributes, such as materials, heating systems, location, and ventilation options, affect thermal comfort [15].

Conventional solar and non-solar air-conditioning tents combine renewable energy with temporary shelter, enhancing outdoor comfort. Air conditioning units in these tents maintain a stable temperature. Efficient air circulation, which means airflow that quickly distributes cooled or heated air, is key to energy savings and user comfort. High-quality thermal insulation materials that slow heat loss or gain, and advanced solar panel technology that uses solar cells to convert sunlight into usable electricity, are essential. Furthermore, materials that retain heat (store warmth for later use), resist fire (are non-flammable), and provide waterproofing (prevent water entry) further ensure safety and comfort [19]. Solar panels exchange sunlight for electrical energy, which powers air conditioning. Other tents use air-supply pipes (ducts that guide air) and ventilation fans (devices that move air) to boost airflow [20].

Although these approaches promise the thermal comfort of conventional solar and non-solar air-conditioning tents, they may also increase the tent's weight, cost, electrical consumption and complexity. This study presents a novel theoretical approach to design a passive solar heating tent that utilises free and renewable solar energy to maintain interior temperatures effectively. Using SolidWorks, we were able to design and simulate this tent, which has a metal base and a Nylon 6.6 cover. Additionally, the tent employs a sustainable passive solar system, making it environmentally friendly. Furthermore, this study highlights the vital effect of the varying aperture area resulting from the sun's trajectory on the energy harvested by the tent.

2. Materials and methods

We designed a four-person tent featuring a passive solar heating system utilising the SolidWorks software. The structure consists of a metal frame; it also features an outer layer made of nylon 6.6 fabric, known for its distinctive properties [21] and commonly utilised in parachutes because of its excellent air insulation. The design comprises a rectangular prism consisting of five containers – passive solar air containers and insulation air containers (PSAC and IAC) that can be assembled in the winter and disassembled in the summer: three coated passive solar air canisters (PSAC) for the walls and two insulating air containers (IAC) for the doorway and roof. PSACs are covered with black

nitrocellulose paint on one external side of each PSAC to improve solar radiation absorption efficiency.

The uncoated sides of these PSACs, on the other hand, feature openings at the top and bottom. The openings at the top and bottom of the tent match with the openings on either side of the containers. All containers are secured to the tent with adhesive tapes bonded to both the tent and the containers. When installed within the tent, each painted side of the containers is oriented towards the east, south and west, respectively, to optimise solar energy collection on their surfaces. Figure 1 (a and b) displays the setting.

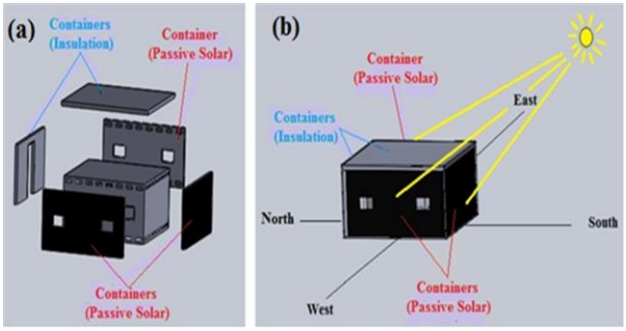


Fig. 1. (a) PSAC and IAC elements, and
(b) PSAC and IAC assembled in the tent.

The tent's entrance is located on the northern side, which is the fourth side. The variation in density will result in the energy absorbed from solar radiation heating the air within the PSAC, causing it to ascend to the top, where it will enter the tent through the upper openings, while cooler air will enter the container through the lower openings. The air circulation system elevates the tent's temperature during the day by employing the thermosiphon principle. This study aims to propose a theoretical design for an emergency tent with a novel solar heating system. This design is ready to be installed at any time, and all necessary mathematical calculations to validate it will be presented.

2.1. Space heating load and harvested energy

The required heating load is calculated by subtracting the heat obtained from occupants and objects within the tent while considering the heat losses through the tent's walls, ceiling and floor, with an internal temperature set at 22°C and an outside temperature of 0°C. The heat losses depend on the air properties, and the thermal resistances (R_t) are displayed in Fig. 2.

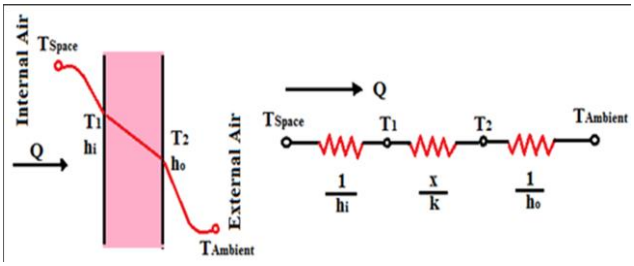


Fig. 2. Thermal resistances across the wall [23].

While the thermal conductivity (k) of the concrete floor equals 1.35 W/(m·K) [22], simultaneously, presuming the soil temperature to be between 10ºC and 14ºC. This study highlights two layers in the ground: the concrete layer (first) and the underlying soil layer (second). It is worth mentioning that this tent can also be set up directly on the ground without the use of a concrete layer.

2.1.1. Total amount of required power (Q_r)

The variation between heat losses (Q_{loss}) and heat gains (Q_{gain}) specifies the quantity of heat that must be supplied to the tent for the heating load (Q_r), which is:

$$Q_r = Q_{loss} - Q_{gain}, \quad (1)$$

where Q_r is the total amount of the required power in W.

- **Energy losses (Q_{loss})**

Load estimation is predicated on the assumption that the energy losses (Q_{loss}) of a tent are directly proportional to the temperature variation between its interior and exterior. In addition, the tent's wall cross sections that face the sun are involved in the calculations; despite the heat gain from the three PSAC, the calculations were based on the maximum thermal losses from the tent's walls, ceiling and floor:

$$Q_{loss} = UA_c(T_{sp} - T_{am}), \quad (2)$$

where A_c denotes the cross-sectional area of each layer. The overall heat transfer coefficient (U) for each element of the outer casing is obtained by the thermal resistance method, which accounts for the resistance of the convectional heat transfer on the inner and outer surfaces and the thermal conductivity resistance of all the layers of the material.

The overall heat transfer coefficient is given by [23]:

$$U = \frac{1}{R_t} = \frac{1}{\frac{1}{h_i} + \sum\frac{x}{k} + \frac{1}{h_o}}, \quad (3)$$

where X is the nylon 6.6 fabric thickness (0.8 mm); the thermal conductivity (k) of nylon used in the walls and roof is 0.25 W/(m·K), whereas the thermal conductivity of air is 0.0257 W/(m·K), the containers' thickness is 15 cm. The floor thickness is specified as 10 cm for concrete and 1 m for soil.

The convection heat transfer coefficient for internal static air is 8.29 W/(m^2·K), while the coefficient for moving air in winter is 34.1 W/(m^2·K) [22].

The total losses can be calculated as:

$$Q_{loss} = Q_1 + Q_2 + Q_3 + Q_4 + Q_5 + Q_6 + Q_7 + Q_{inf}, \quad (4)$$

Taking into account thermal losses: through the tent walls (Q_1, Q_2, Q_3), windows (Q_4), door (Q_5), ceiling (Q_6), floor (Q_7), and through infiltration (Q_{inf}). The notations (1−7) correspond to the values of A_c listed in Table 1.

- **Energy gain (Q_{gain})**

Persons residing in air-conditioned environments experience a loss of sensible heat that fluctuates according to their condi-

tion. This occurs because their bodies release heat when exposed to the tent's inner air, which is at 37°C. Furthermore, latent heat is generated from sweat on the body's surface and the evaporation of water in the lungs, which contributes thermal energy and decreases the heating load, along with the heat gain from electrical equipment:

$$Q_{gain} = Q_P + Q_e. \quad (5)$$

The sensible heat gained by individuals (Q_S) can be calculated using the equation [22]:

$$Q_S = N_P H_S CLF. \quad (6)$$

In refrigeration calculations, *CLF* denotes the cooling load factor, but in this context, it refers to the heat gain load factor per person. The value of H_s is dependent upon the person's activities within the tent and its magnitude. The latent heat gain from occupants (Q_l) in a space is expressed by the subsequent equation:

$$Q_l = N_P H_l . \quad (7)$$

H_l denotes the latent heat rate for an individual within the space, with its value dependent upon the nature of the person's activity.

The total heat gain due to the presence of people inside the tent (Q_p) was calculated from the following equation:

$$Q_P = Q_S + Q_l, \quad (8)$$

When calculating the heat gain load from equipment in the tent, references equate this gain to the power consumption of the devices, taking into account usage factors, and calculate the heat gains as follows [22]:

$$Q_e = P_e F_u F_{hg}, \quad (9)$$

where Q_e is the heat gain from equipment (W), P_e is the equipment power (W), F_u is the usage factor

$$F_u = \frac{Actual\ operating\ time}{Design\ period}; \quad (10)$$

F_{hg} is the heat gain factor, and the design period is 10 hours.

2.2. The main components of the tent and solar heating system

2.2.1. The main metal structure assembly

Figure 3 illustrates a primary metal framework of the tent (of size 4 m × 4 m × 2 m) designed for fast assembly and disassembly, which utilises metal assemblies secured at each of its eight corners with screws and nuts. The subsequent assemblies are as follows: for each tent, two symmetrical side metal components, fabricated from 40 mm × 40 mm × 1.25 mm square hollow section tubes, are employed. The symmetrical complexes on the right and left are interconnected at the top by ribs made of a square hollow section, with bond plates at the ends that attach the components affixed to the aforementioned complexes.

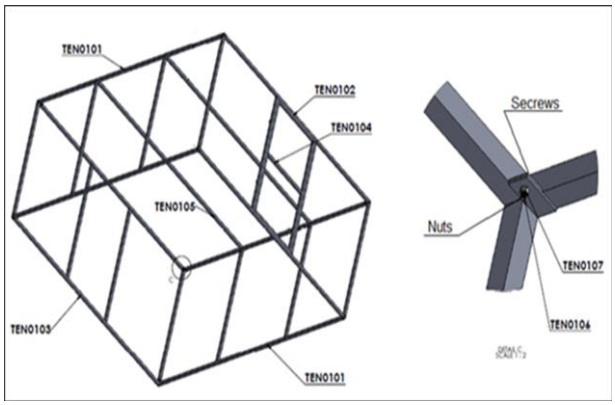


Fig. 3. The tent metal assemblies and their connections.

The next phase includes affixing the door frame to the primary construction of the tent utilising a door hinge. Subsequently, a body constructed from nylon 6.6 fabric is sewn and positioned over the framework in accordance with Fig. 4.

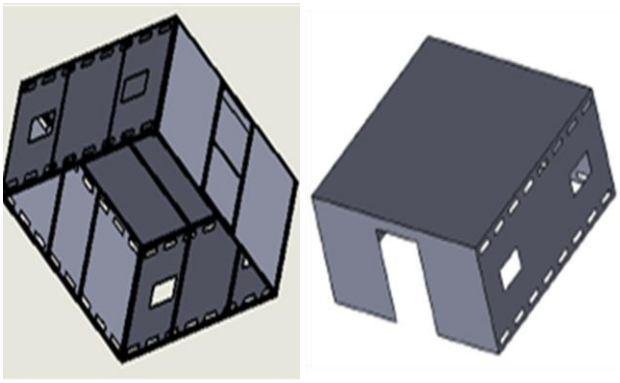


Fig. 4. The fabric framework of the tent.

Finally, the door fabric is attached to the door structure and metal frame using connecting belts and a fabric label. This connection allows air to pass between the frame and the fabric, effectively eliminating the effect of heat conduction between them.

2.3. PSAC and IAC

During this step, we have connected PSAC, specifically the left, right and rear, along with IAC for the door and roof. This procedure is illustrated in Fig. 5, which depicts the connections using belts and fabric sticker labels around the windows and their edges. PSAC and IAC are equipped with valves for the primary purpose of air filling. In order to take the form of a parallel rectangular shape, it employs an assembly of plastic tubes (2" C.P.V.C SCH 80) as illustrated in Fig. 6 to maintain their shapes by linking them at the outer corners and ends of the containers (PSAC and IAC), as depicted in Fig. 5.

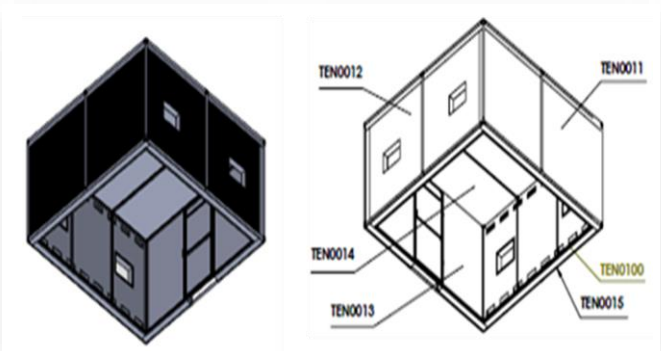


Fig. 5. Tent structure incorporating PSAC and IAC with CPVC tubing assembly.

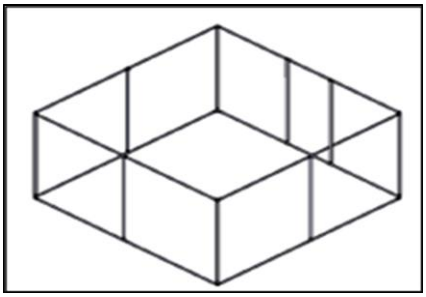


Fig. 6. Outer support tube assembly.

2.4. Sun trajectory calculations

Static solar containers (PSACs) capture solar radiation through their variable aperture area, defined as the section of PSAC oriented toward the sun that receives incident solar radiation. This mechanism controls the amount of solar energy harvested. The aperture area of PSAC varies from sunrise to sunset as the solar angles (azimuth and elevation) change. To compute the changing aperture of three PSACs facing the sun as a function of elevation and azimuth solar angles, the following mathematical relation was developed, Eq. (11):

$$A_a\,(z,\alpha) = L\cos(90+Z)\,2\cos(90-\alpha) + \\ +W\cos(Z)\,2\cos(\alpha). \quad (11a)$$

When subtracting the area of the tent windows, the equation becomes as follows:

$$A_a\,(z,\alpha) = L\cos(90+Z)\,2\cos(90-\alpha) + \\ -2l\cos(90+Z)\,w\cos(90-\alpha) + \\ +W\cos(Z)\,2\cos(\alpha). \quad (11b)$$

where Z denotes the azimuth angle, α represents the elevation angle. L and W indicate the length and height of PSAC, while l and w identify the length and height of the windows. The elevation angle (α) is determined according to [24]:

$$\alpha = sin^{-1}(\cos(Lat)\cos(\delta)\cos(th) + \sin(Lat)\sin(\delta)), \quad (12)$$

where th is the time hour angle, Lat is the position's latitude (33.27°), and δ is the declination. These parameters can be determined as [24–27]:

$$\delta = 23.45\sin\left(\frac{360}{365}(284+n)\right), \quad (13)$$

where n represents the number of the day within the year, and

$$th = 15(ST-12). \quad (14)$$

The solar time (ST) can be determined from [19]:

$$ST = LT + 4(Lon - STM) + EoT, \quad (15)$$

where LT is the local time, Lon is the local longitude (44.4°E), STM is the standard time meridian (45°E), EoT is the equation of time, which reads as [28]:

$$EoT = 9.87\sin(2\beta) - 7.53\cos(\beta) - 1.5\sin(\beta), \quad (16)$$

$$\beta = \frac{360}{364}(n-81), \quad (17)$$

$$Z = \arcsin(\sec(\alpha)\cos(\delta)\ \sin(th)). \quad (18)$$

3. Results and discussion

3.1. Energy losses and energy gain

- **Energy losses (Q_{loss})**

First, we have to set the values for the overall heat transfer coefficients using Eq. (3): U_1 = 0.168 W/(m²·K) for the right, left and rear walls and also for the door wall and ceiling, U_2 = 6.5 W/(m²·K) for the door, U_3 = 6.27 W/(m²·K) for the windows, U_4 = 5.14 W/(m²·K) for the floor.

Using Eq. (2) to calculate the heat losses yields the results presented in Table 1 for the floor concrete thickness of 10 cm and for dry soil of thickness 1 m (effective depth).

Table 1. Details of heat losses calculations.

Heat losses	Cross section area, m²	Values, W	Details
Q_1	7.52	55.58	right and left tent walls
Q_2	8	29.6	rear wall
Q_3	6.2	22.9	door wall
Q_4	0.96	132.4	windows
Q_5	1.8	257.4	door
Q_6	16	59.1	ceiling
Q_7	16 16	822.4 80	floor (concrete) floor (dry soil)

Note that the air infiltration ($\dot{Q}_{inf}$) is a contributing factor to heat loss and can be calculated using the method [22]:

$$\dot{Q}_{inf} = 1.22\,\dot{V}(T_{sp} - T_{am}), \quad (19)$$

where $\dot{V}$ represents the volumetric rate of air exchange, determined as:

$$\dot{V} = \frac{V\,n}{3600}. \quad (20)$$

The value *n* indicates the quantity of air changes. Assuming one-time air change (1), *V* represents the volume of a tent covering 32 m³. Applying the preceding formula, we derive:

$$\dot{V} = 0.00889 \text{ m}^3/\text{s}.$$

By substituting values of T_{sp} = 22°C and T_{am} = 0°C into Eq. (19), we obtain:

$$\dot{Q}_{inf} = 238.8 \text{ W}.$$

Placing the data from Table 1 and $\dot{Q}_{inf}$ into Eq. (4) gives:

$$Q_{loss} = 1618 \text{ W}.$$

- **Energy gain (Q_{gain})**

In the context of minor activities such as sitting or light work, the *CLF* value is 0.65, while the *CLF* value varies according to the duration of an individual's presence, with a range of 0.5−0.79 for a 4-hour presence [22]. Inputting the values of H_S, *CLF* and the number of individuals, *NP*, into the aforementioned Eq. (6) yields:

$$Q_s = 182 \text{ W}.$$

In addition, for sitting or light work, H_l is measured at 55 W [22]. Substituting values of H_l and the number of individuals into Eq. (7) yields:

$$Q_l = 220 \text{ W}.$$

Finally, substituting the values of Q_S and Q_l into Eq. (8) results in:

$$Q_P = 402 \text{ W}.$$

Assuming that the devices operate at completely full power, the heat gain factor is equal to 1, and the usage factor is based on actual operating time of the equipment. The calculations of the heat gain by the equipment using Eq. 9 are detailed in Table 2. The total heat gain by the equipment is 216 W.

Table 2. Details of the heat gain load for the equipment.

Equipment	Device number	Total Power, W	Actual operating time, h	Usage factor	Heat gain, W
Laptop and charger	2	130	4	0.4	52
Mobile charger	4	40	0.5	0.05	2
Kettle	1	2000	0.5	0.05	100
Monitor LED	1	70	6	0.6	42
Lighting LED	2	20	10	1	20

By substituting values of Q_p = 402 W and Q_d = 216 W in Eq. (5), we obtained the following:

$$Q_{gain} = 618 \text{ W}.$$

3.2. Total amount of required power (Q_r)

From Eq. (1): Q_r = 1000 W. Now the total energy (Q_t) required to heat the tent for a duration of 10 hours is as follows:

$$Q_t = Q_r \times \textit{used hours of day}, \quad (21)$$

$$Q_t = 1000 \times 10 \text{ hours} \times 3600 = 36000 \text{ kJ} = 10 \text{ kWh}.$$

3.3. Harvested energy and optical calculations

The energy collected from the sun via the PSAC is called harvested energy (Q_h). This energy can be expressed as:

$$Q_h = I\, A_a\, \eta. \quad (22)$$

To find the minimum aperture area (A_a) of the passive solar energy collector that must be exposed to solar radiation to meet the required load (as much as possible), we must assume that the calculated total energy (36000 kJ) is equal to the harvested energy (Q_h). Now:

$$A_a = \frac{Q_t}{I\eta}. \quad (23)$$

Between October and March, the average solar radiation for the winter, over a six-month duration of 10 hours daily, is 3.868 kWh/m² [29]. The absorptance of the black paint (cellulose nitrate) is 0.78, representing η [30]. Consequently, the required aperture area for the passive solar collector is:

$$A_a = \frac{10 \text{ kWh}}{3.868 \text{ kWh/m}^2 \text{ x } 0.78} = 3.31 \text{ m}^2.$$

Applying a cumulative method with spatial adjustments based on the sun's trajectory (azimuth and elevation) as detailed in Eqs. (11)−(18), Table 3 presents the amount of harvested energy obtainable over a nine-hour period. Measurements were recorded every ten minutes (see the appendix); however, for simplicity, the data presented in Table 3 represents hourly averages throughout the day. The coordinates for Baghdad, Iraq (33.27°N, 44.38°E) were employed in the calculations.

Table 3. The detailed data of harvested energy and actual aperture area with corresponding azimuth and elevation angles for every hour.

Time, hh:mm	Azimuth, deg.	Elevation, deg.	Aperture area, m²	Solar radiation, W/m²	Energy, kJ
07:30 a.m.	−58.16	4.42	4.71	19	-
08:30 a.m.	−48.64	14.49	6.54	169	1508.3
09:30 a.m.	−37.24	23.05	7.65	300	4727.8
10:30 a.m.	−23.62	29.42	7.87	400	7832.4
11:30 a.m.	−8.04	32.85	7.23	454	9167.5
12:30 p.m.	8.35	32.82	7.23	454	9015.0
01:30 p.m.	23.90	29.32	7.87	403	9239.6
02:30 p.m.	37.48	22.90	7.65	311	7949.3
03:30 p.m.	48.84	14.31	6.54	174	4981.7
04:30 p.m.	58.33	4.22	4.71	21	1497.2

Since the outside air temperature was assumed to be 0°C and the inside tent temperature was 22°C, we could calculate the required heating load by calculating the tent's thermal losses. According to Eq. (21), the calculations produced a heating energy load of 36 000 kJ. If the indoor temperature rises above 22°C, the windows can be opened to maintain the desired value.

On December 21, the shortest day of the year, which produces the least amount of energy during the winter, the accumulation approach can be used to measure the outcome at 10-minute intervals [31].

Figure 7 depicts the variation in the aperture area (Col. Area) as it correlates with changes in azimuth (Azm.) and elevation (Elev.) throughout the day.

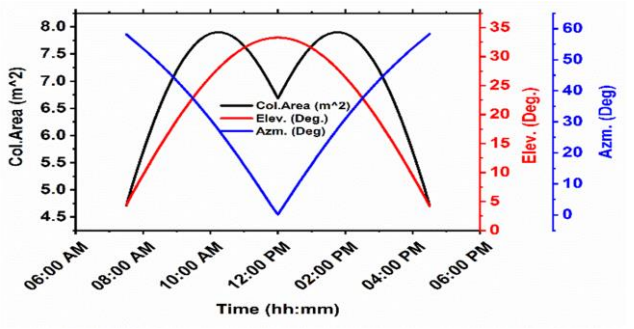


Fig. 7. The correlation involving aperture area, elevation and azimuth.

Figure 7 demonstrates that while elevation and azimuth varies throughout the day, the actual aperture area consistently exceeds its minimum calculated value of 3.31 m^2, indicating that the energy collected would be greater than the requirements for space heating.

Figure 8 illustrates the variation in aperture area in connection with variations in azimuth and elevation over a half-day period (from 7:30 a.m. to 12:00 p.m.). The identical occurrence is expected to take place throughout the forthcoming half-day (from 12:00 p.m. to 4:30 p.m.). The changing aperture area and the intensity of solar radiation will influence the efficiency of energy harvested from PSAC. The section of the aperture area curve depicted in Fig. 8 aligns with the Gaussian model, as illustrated within the figure.

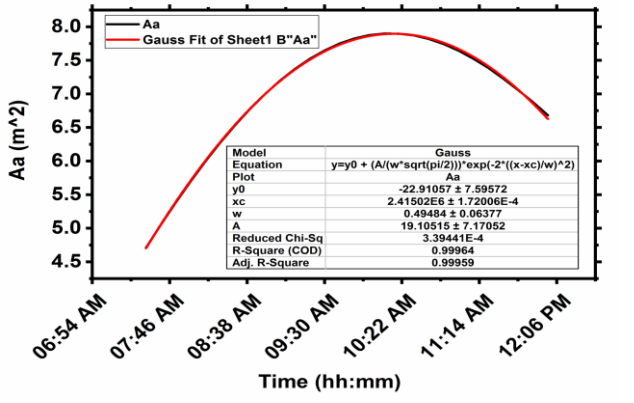


Fig. 8. Behaviour of aperture area variation with Gauss model fitting.

By employing Eq. (22), we can compute how much energy the PSAC captured from the sun's rays for the entire shortest winter day, as illustrated in Fig. 9. The result was 55 919.04 kJ. The solar radiation data for December 21 demonstrate the effect of changes in the aperture area (A_a) and solar radiation (S. Rad.) values on the quantity of harvested energy produced, as shown in Fig. 9.

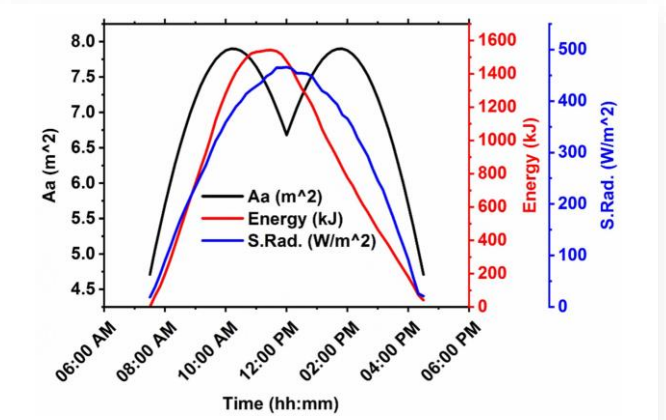


Fig. 9. The influence of aperture area and solar radiation on the energy harvested.

At 10:10 a.m., the maximum aperture area was measured as 7.898 m^2, with solar radiation recorded at 374 W/m^2, resulting in an energy gain of 1352.7 kJ. The highest recorded energy was 1542.44 kJ at 11:30 a.m. The aperture area measured 7.23 m^2 under solar radiation of 454 W/m^2. This variation arises from the simultaneous influence of aperture areas and solar radiation values on the energy obtained.

6. Conclusions

The project aimed to develop an innovative technique for designing an emergency passive solar heating tent that utilises renewable and cost-free solar energy to maintain appropriate internal temperatures.

The research demonstrates that a tent measuring 4 m × 4 m × 2 m can accommodate up to four people while providing the necessary space-heating load and usable solar energy. Another advantage of the tent is the simplicity of assembly and disassembly. The aperture area of PSAC, which varies throughout the day as the sun traverses the sky, determines the amount of energy that may be harvested.

This design simulation focuses only on the volumetric rate of air exchange and assumes one-time air change for simplicity.

Additional practical parameters, such as wind speed, pressure differences, air temperature differences and minimum ventilation, could influence the calculation of the heat losses. All these parameters will be taken into account in our future work.

References

[1] Davis, I. (1978). *Shelter after disaster*. UNESDOC Digital Library, Oxford Polytechnic Press.

[2] Poschl, R.A. (2017). *Modelling the thermal comfort performance of tents used in humanitarian relief*. Ph.D. dissertation, Loughborough University.

[3] Banks, B. A. (2024). *Write to Return: Huguenot Refugees on the Frontiers of the French Enlightenment*. McGill-Queen's Refugee and Forced Migration Studies, Vol. 14.

[4] Hantscher, S. (2019). The UNHCR and Environmentally Displaced Persons. In *The UNHCR and Disaster Displacement in the 21st Century: An Organizational Analysis* (pp. 119–192). Springer. doi: 10.1007/978-3-030-19689-9_5

[5] Murray, L. (2015). Sheltering from disaster. *Engineering & Technology*, 10(1), 58−61. doi: 10.1049/et.2015.0107

[6] Gentile, V., Nigra, M., Simonetti, M., & Perino, M. (2025). Design and testing of an emergency humanitarian tent for airborne risk mitigation with natural ventilation. *E3S Web of Conferences*, 672, 01006. doi: 10.1051/e3sconf/202567201006

[7] Cao, K., Lan, M., Wang, H., Li, Y., & Liu, X. (2023). The thermal environment and thermal comfort of disaster relief tents in high-temperature composite environment. *Case Studies in Thermal Engineering*, 50, 103453. doi: 10.1016/j.csite.2023.103453

[8] Ullal, A., Aguacil, S., Vannucci, R., Yang, S., Pernot, J.G., Licina, D., & Tombesi, P. (2022). Comparing thermal performance of standard humanitarian tents. *Energy and Buildings*, 264, 112035. doi: 10.1016/j.enbuild.2022.112035

[9] Matusiak, M. (2010). Thermal comfort index as a method of assessing the thermal comfort of textile materials. *Fibres & Textiles in Eastern Europe*, 18(2), 45–50.

[10] Rupp, R.F., Vásquez, N.G., & Lamberts, R. (2015). A review of human thermal comfort in the built environment. *Energy and Buildings*, 105, 178–205. doi: 10.1016/j.enbuild.2015.07.047

[11] De Dear, R.J., Akimoto, T., Arens, E.A., Brager, G., Candido, C., Cheong, K.W.D., & Zhu, Y. (2013). Progress in thermal comfort research over the last twenty years. *Indoor air*, 23(6), 442–461. doi: 10.1111/ina.12046

[12] Susanti, L. (2015). Thermal comfort evaluation of emergency tent using PMV and PPD model. In *Proceedings of the International Multi Conference of Engineers and Computer Scientists* (pp. 958−963), March 18–20, Hong Kong.

[13] Nicol, F., Humphreys, M., & Roaf, S. (2012). *Adaptive thermal comfort: principles and practice* (1st ed.). Routledge, London. doi: 10.4324/9780203123010

[14] Yang, H., Jiang, Y., Liu, J., & Gong, Z. (2016). The field investigation on thermal comfort of tent in early autumn of Tianjin. *MATEC Web of Conferences*, 61, 01001. doi: 10.1051/matecconf/20166101001

[15] Potangaroa, R., & Hynds, M. (2008). Thermal comfort tools for emergency shelter in major disasters. *Proceedings from CIB International Conference on Building Education and Research, School of the Built Environment* (pp. 1457–1472), 11–15 February 2008, Heritance Kandalama, Sri Lanka.

[16] Zemitis, J., Borodinecs, A., Bogdanovics, R., & Geikins, A. (2021). A case study of thermal comfort in a temporary shelter. *Journal of Sustainable Architecture and Civil Engineering*, 29(2), 139–149. doi: 10.5755/j01.sace.29.2.29240

[17] Yousef, M. (2023). More humane engineering ideas for the design of shelter units (camps) Renewable Energy Produced Tent Idea (weaving a home). *International Journal of Advanced Engineering and Business Sciences*, 4(3). doi: 10.21608/ijaebs.2023.210485.1083

[18] Butcher, K., & Craig, B. (Eds.). (2015). *Guide A Environmental design* (8th ed.). Chartered Institution of Building Services Engineers, London.

[19] Guangliang, H. (2012). *Solar air-conditioning tent*. China Patent CN 102400589 A, 04 April. https://lens.org/001-926-548-381-407 [accessed 22 Feb. 2026].

[20] Dai, M. (2014). *Solar ventilation-type tent*. China Patent CN 203394150 U, 15 January. https://lens.org/117-693-182-419-301 [accessed 22 Feb. 2026].

[21] King, J.A., Tucker, K.W., Vogt, B.D., Weber, E.H., & Quan, C. (1999). Electrically and thermally conductive nylon 6.6. *Polymer Composites*, 20(5), 643–654, doi: 10.1002/pc.10387

[22] Owen, M.S. (Ed.). (2009). *The 2009 ASHRAE Handbook: Fundamentals*. American Society of Heating. American Society of Heating, Refrigerating and Air-Conditioning Engineers

[23] Holman, J.P. (2010). *Heat transfer*. 10th ed. McGraw-Hill Series in Mechanical Engineering, Boston.

[24] Chen, X.M., Li, Y., Zhao, Z.G., Ma, T., & Wang, R.Z. (2018). General method to obtain recommended tilt and azimuth angles for photovoltaic systems worldwide. *Solar Energy*, 172, 46–57. doi: 10.1016/j.solener.2018.06.045

[25] Shivalingaswamy, T., & Kagali, B.A. (2012). Determination of the Declination of the Sun on a Given Day. *European Journal of Physics Education*, 3(1), 17−22.

[26] Abdurrahman, M., Gambo, J., Shitu, I.G., Yusuf, Y.A., Dahiru, Z., Idris, A.M., & Isah, A.A. (2019). Solar elevation angle and solar culmination determination using celestial observation; a case study of hadejia jigawa state, Nigeria. *International Journal of Advances in Scientific Research and Engineering*, 5(9), 8−17. doi: 10.31695/IJASRE.2019.33482

[27] Sproul, A. B. (2007). Derivation of the solar geometric relationships using vector analysis. *Renewable Energy*, 32(7), 1187−1205, doi: 10.1016 /j.renene. 2006. 05.001

[28] Duffie, J.A., Beckman, W.A., & Blair, N. (2020). *Solar engineering of thermal processes, photovoltaics and wind*. John Wiley & Sons.

[29] Ahmed, B.K., Younis, G.G., & Abdalwahid, Z. (2021). Estimation and Analysis of Solar Radiation on Horizontal and Inclined Surface for Baghdad City. *Iraqi Journal of Science*, 62(11), 4249–4259. doi: 10.24996/ijs.2021.62.11(SI).5

[30] Mutlak, F. (2011). *Design and fabrication of parabolic trough solar collector for thermal energy applications*. Ph.D. Thesis, University of Baghdad.

[31] Abdulla, F.M. (2019). Calculating the variations of sunrise, sunset and day length times for Baghdad city with comparison to different regions of the world in year 2019. *Iraqi Journal of Science*, 62(12), 2732–2741. doi: 10.24996/ijs.2019.60.12.24

Appendix

Table 4 presents the results of calculations of the harvested energy every ten minutes, along with the effects of azimuth and elevation on the aperture area and amount of energy harvested.

Table 4. The detailed data of harvested energy and actual aperture area every ten minutes with corresponding azimuth and elevation angles.

Time, hh:mm	Azimuth, deg.	Elevation, deg.	Aperture area, m²	Solar radiation, W/m²	Energy, kJ
07:30 AM	−58.16	4.42	4.71	19	-
07:40 AM	−56.68	6.19	5.05	38	65.11
07:50 AM	−55.17	7.91	5.38	63	123.34
08:00 AM	−53.60	9.61	5.70	90	198.38
08:10 AM	−51.10	11.28	5.10	116	281.88
08:20 AM	−50.35	12.90	6.27	143	371.90
08:30 AM	−48.64	14.49	6.54	169	467.74
08:40 AM	−46.88	16.04	6.78	192	562.44
08:50 AM	−45.08	17.54	6.10	213	652.80
09:00 AM	−43.20	18.10	7.19	234	742.30
09:10 AM	−41.28	20.40	7.37	254	831.67
09:20 AM	−39.29	21.75	7.52	274	919.93
09:30 AM	−37.24	23.05	7.65	300	1018.70
09:40 AM	−35.12	24.28	7.75	323	1122.28
09:50 AM	−32.96	25.45	7.82	340	1208.05
10:00 AM	−30.71	26.55	7.87	359	1283.91
10:10 AM	−28.41	27.58	7.898	374	1352.70
10:20 AM	−26.05	28.54	7.896	389	1410.05
10:30 AM	−23.62	29.42	7.87	400	1455.43
10:40 AM	−21.14	30.21	7.82	414	1494.01
10:50 AM	−18.62	30.92	7.74	422	1521.93
11:00 AM	−16.03	31.55	7.64	429	1531.93
11:10 AM	−13.40	32.08	7.52	436	1535.09
11:20 AM	−10.74	32.51	7.38	448	1542.14
11:30 AM	−8.04	32.85	7.23	454	1542.44
11:40 AM	−5.31	33.10	7.06	465	1536.25
11:50 AM	−2.59	33.24	6.87	465	1516.05
12:00 PM	0.16	33.29	6.68	466	1476.56
12:10 PM	2.90	33.23	6.875	463	1473.39
12:20 PM	5.63	33.08	7.06	454	1494.86
12:30 PM	8.35	32.82	7.23	454	1517.87
12:40 PM	11.05	32.47	7.38	453	1550.10
12:50 PM	13.70	32.02	7.52	448	1571.80
01:00 PM	16.33	31.48	7.64	433	1563.48
01:10 PM	18.90	30.85	7.74	420	1535.53
01:20 PM	21.43	30.13	7.82	414	1518.29
01:30 PM	23.90	29.32	7.87	403	1499.52
01:40 PM	26.33	28.43	7.90	393	1468.34
01:50 PM	28.67	27.47	7.90	373	1415.60
02:00 PM	30.97	26.43	7.87	366	1363.77
02:10 PM	33.20	25.32	7.82	350	1315.13
02:20 PM	35.37	24.15	7.75	328	1235.38
02:30 PM	37.48	22.90	7.65	311	1151.10
02:40 PM	39.52	21.60	7.52	293	1071.94
02:50 PM	41.50	20.25	7.37	268	977.43
03:00 PM	43.42	18.83	7.19	245	874.27
03:10 PM	45.28	17.37	6.10	228	785.47
03:20 PM	47.08	15.87	6.78	200	689.87
03:30 PM	48.84	14.31	6.54	174	582.69
03:40 PM	50.54	12.72	6.30	146	479.73
03:50 PM	52.18	11.09	5.10	119	380.51
04:00 PM	53.78	9.42	5.70	92	288.72
04:10 PM	55.34	7.72	5.38	57	193.19
04:20 PM	56.85	5.99	5.05	26	101.36
04:30 PM	58.33	4.22	4.71	21	53.69